




## ARTICLE

# Process-induced cell cycle oscillations in CHO cultures: Online monitoring and model-based investigation

Johannes Möller<sup>1</sup>  | Krathika Bhat<sup>1</sup> | Kristoffer Riecken<sup>2</sup> | Ralf Pörtner<sup>1</sup>  |  
An-Ping Zeng<sup>1</sup> | Uwe Jandt<sup>1</sup> 

<sup>1</sup>Bioprocess and Biosystems Engineering,  
Hamburg University of Technology, Hamburg,  
Germany

<sup>2</sup>Department of Stem Cell Transplantation,  
Research Department Cell and Gene Therapy,  
University Medical Centre (UMC) Hamburg-  
Eppendorf, Hamburg, Germany

## Correspondence

Uwe Jandt, Hamburg University of  
Technology, Institute of Bioprocess and  
Biosystems Engineering, Denickestr. 15, K-  
1567, 21073 Hamburg, Germany.  
Email: uwe.jandt@tuhh.de

## Funding information

Bundesministerium für Bildung und  
Forschung, Grant/Award Number: 031B0222;  
Deutsche Forschungsgemeinschaft, Grant/  
Award Number: ZE 542/91

## Abstract

The influence of process strategies on the dynamics of cell population heterogeneities in mammalian cell culture is still not well understood. We recently found that the progression of cells through the cell cycle causes metabolic regulations with variable productivities in antibody-producing Chinese hamster ovary (CHO) cells. On the other hand, it is so far unknown how bulk cultivation conditions, for example, variable nutrient concentrations depending on process strategies, can influence cell cycle-derived population dynamics. In this study, process-induced cell cycle synchronization was assessed in repeated-batch and fed-batch cultures. An automated flow cytometry set-up was developed to measure the cell cycle distribution online, using antibody-producing CHO DP-12 cells transduced with the cell cycle-specific fluorescent ubiquitination-based cell cycle indicator (FUCCI) system. On the basis of the population-resolved model, feeding-induced partial self-synchronization was predicted and the results were evaluated experimentally. In the repeated-batch culture, stable cell cycle oscillations were confirmed with an oscillating G1 phase distribution between 41% and 72%. Furthermore, oscillations of the cell cycle distribution were simulated and determined in a (bolus) fed-batch process with up to  $25 \times 10^6$  cells/ml. The cell cycle synchronization arose with pulse feeding only and ceased with continuous feeding. Both simulated and observed oscillations occurred at higher frequencies than those observable based on regular (e.g., daily) sample analysis, thus demonstrating the need for high-frequency online cell cycle analysis. In summary, we showed how experimental methods combined with simulations enable the improved assessment of the effects of process strategies on the dynamics of cell cycle-dependent population heterogeneities. This provides a novel approach to understand cell cycle regulations, control cell population dynamics, avoid inadvertently induced oscillations of cell cycle distributions and thus to improve process stability and efficiency.

## KEYWORDS

automated flow cytometry, fed-batch, feeding strategy, FUCCI, repeated-batch

**Abbreviations:** Abbreviation, Explanation; Acf, putative autocrine factor; AFC, automated Flow Cytometry; Amm, ammonium; CHO, Chinese hamster ovary; DAPI, 4,6-diamidin-2-phenylindol; FITC-A, fluorescein isothiocyanate filter in flow cytometry; FUCCI, fluorescent ubiquitination-based cell cycle indicator; FSC, forward scatter; Gln, glutamine; Glc, glucose; Lac, lactate; Ab, antibody; PBS, phosphate buffered saline; SSC, side scatter; TCA, tricarboxylic acid cycle.

This is an open access article under the terms of the Creative Commons Attribution License, which permits use, distribution and reproduction in any medium, provided the original work is properly cited.

© 2019 The Authors. *Biotechnology and Bioengineering* published by Wiley Periodicals, Inc.

| Nomenclature     |  |            |
|------------------|--|------------|
| Variable         | Explanation                                      | Unit       |
| $c_i$            | Concentration of the component $i$               | [mM]       |
| $c_{Glc,F}$      | Glucose concentration in feed                    | [mM]       |
| $c_{Gln,0}$      | Initial glutamine concentration repeated-batch   | [mM]       |
| $c_{Gln,F}$      | Glutamine concentration in feed                  | [mM]       |
| $c_{Gln,ME}$     | Glutamine concentration after medium exchange    | [mM]       |
| $F_{Rate}$       | Feed rate  | [ml/min]   |
| $F_{Start}$      | Start of feed                                    | [h]        |
| $i$              | Glc, Gln, Lac, Amm, Ab, Acf                      | [-]        |
| $i_{red}^n$      | Ratio of fluorescent ratios                      | [%]        |
| $k_i$            | Substrate-specific growth rate                   | [-]        |
| $K_{Gln,\Omega}$ | Dimensionless cell cycle-specific scaling factor | [-]        |
| $mKO_2^n$        | Number of mKO <sub>2</sub> positive cells        | [cells]    |
| $mVenus^n$       | Number of mVenus positive cells                  | [cells]    |
| $p$              | Significance factor                              | [-]        |
| $t$              | Time   | [h]        |
| $t_{ME}$         | Time medium exchange                             | [h]        |
| $V_{\%,ME}$      | Replaced medium                                  | [%]        |
| $X_v$            | Viable cell density                              | [cells/ml] |
| $X_{v,0}$        | Initial viable cell density                      | [cells/ml] |
| $\Omega$         | Cell-cycle states (G1, S, G2/M, and dead cells)  | [-]        |

## 1 | INTRODUCTION

Changes in the cell populations of mammalian cell cultures have received increasing attention. So far, variations in cell populations have been identified in cell line generation (Patel et al., 2018; Scarcelli et al., 2018) and clonal long term stability (Chusainow et al., 2009; Vcelar et al., 2018). To assess heterogeneities under bioreactor cultivation conditions, a combined workflow was developed using near-physiological cell cycle synchronization (review see Jandt, Platas Barradas, Pörtner, & Zeng, 2014) and population-resolved modeling (Jandt, Platas Barradas, Pörtner, & Zeng, 2015; Möller, Korte, Pörtner, Zeng, & Jandt, 2018). Using this approach, strong metabolic up- and downregulation with changing productivities were identified during the cell cycle of nonproducing CHO K1 and

AGE1.hn<sub>ATT</sub> (Jandt et al., 2015) cells and antibody-producing Chinese hamster ovary (CHO) cells (Möller et al., 2018). However, it is still not understood, to which extent bulk process conditions can trigger, amplify or damp cell cycle oscillations in otherwise nonsynchronized cultures under near-production conditions. This knowledge would be helpful to either intentionally synchronizes cultures without physical selection (e.g., elutriation; Cooper & Gonzalez-Hernandez, 2009), or to avoid any undesired oscillation of the cell cycle distribution by choosing appropriate conditions. The investigation of such processes requires a mathematical process model to determine the suitable conditions and highly time-resolved data sets of the cell cycle progression in the bioreactor, ideally obtained online.

We recently showed that the genetic integration of the fluorescent ubiquitination-based cell cycle indicator (FUCCI) system (originally developed by Sakaue-Sawano et al., 2008) can be applied to the online monitoring of the cell cycle distribution of CHO-K1 cells (Fuge, Hong, Riecken, Zeng, & Jandt, 2017). In brief, two fluorescent molecules representing either the G1 phase (mKO<sub>2</sub>-red) or the S/G2/M phases (mVenus-green) are expressed and degraded according to the cell cycle.

In this study, an automated and online flow cytometry set-up was designed and a population-resolved model was used to predict and assess the population dynamics of CHO cells under variable process conditions. For this, antibody-producing CHO cells were lentivirally transduced with the FUCCI system. The online set-up was used to measure the actual cell cycle status of individual cells with a sufficiently high frequency (i.e., every few hours), thus providing details on the dynamics of process-induced cell cycle oscillations. The model parameters derived in a previous study (Möller et al., 2018) were used to estimate process parameters for the induction of cell cycle oscillations in a repeated-batch and a (bolus) fed-batch cultivation. Experiments were performed with the pre-determined process parameters and cell cycle measurements were carried out online. The crucial model parameters were readjusted based on experimental data. A fed-batch with continuous feeding was used as a negative control. This workflow enables the understanding of cell cycle dependencies and allows to assess and develop cell cycle-dependent bioprocesses without the need for external synchronization techniques. Furthermore, this study demonstrates how cell cycle fluctuations can be inadvertently induced by commonly used pulse feeding strategies, potentially leading to undesired oscillations and thus unpredicted bioprocess behavior.

## 2 | MATERIALS AND METHODS

The aim of this study was to gain an understanding of process-induced oscillations of cell cycle distribution. The basis of the processes (repeated-batch and fed-batch) was a population-resolved model, which describes cell cycle-dependent growth and metabolism of mammalian cells (Jandt et al., 2015; Möller et al., 2018). Materials and methods are partially based on

previous publications for the FUCCI-transduced, nonproducing mammalian cell line derivatives CHO-K1 FUCCI CN and CHO-K1 FUCCI CM (Fuge et al., 2017) and the model-based identification of cell cycle-dependent population dynamics in mammalian cell lines (Castillo, Fuge, Jandt, & Zeng, 2012; Jandt et al., 2015; Möller et al., 2018; Platas Barradas et al., 2015).

## 2.1 | Cell cycle-based fluorescence with FUCCI system

Sakaue-Sawano et al. (2008) developed the FUCCI system, which is based on the cell cycle-dependent expression of two fluorescent proteins, namely mKO<sub>2</sub> and mVenus (Newman & Zhang, 2008; Sakaue-Sawano et al., 2008). mKO<sub>2</sub> was fused to parts of the chromatin licensing and DNA replication factor 1 (30/120; mKO<sub>2</sub>-hCdt1(30/120)) and mVenus to a fragment of the DNA replication inhibitor hGeminin (1/60) (mVenus-hGeminin (1/60)). hCdt1 is mainly expressed during the G1 cell cycle phase whereas hGeminin is absent during this phase. hGeminin is formed during the S/G2/M phases and also acts as an inhibitor to hCdt1. FUCCI-transduced cells express the corresponding fluorescent proteins and change their fluorescence signal due to the cell cycle. The main applications have so far been in the field of tissue growth (Iimura & Lee, 2017; Schoors et al., 2015) and stem cell research (Deglincerti, Etoc, Ozair, & Brivanlou, 2016; Jang et al., 2016).

### 2.1.1 | Generation of FUCCI-derived cell line derivatives

Suspension-adapted CHO DP-12 cells (clone #1934, ATCC CRL-12445, kindly provided by T. Noll, Bielefeld University, Germany) producing an anti-interleukin-8 IgG were cultivated in chemically defined, animal component-free TC-42 medium (Xell AG, Germany). The medium was supplemented with 0.1 mg/L LONG R3 IGF-1, 6 mM glutamine and 200 nM methotrexate (all Sigma-Aldrich, Germany). Exponentially growing CHO DP-12 cells were transduced with lentiviral particles containing the FUCCI construct, which were kindly supplied by the group of Dr. A. Miyawaki (Laboratory for Cell Function Dynamics, RIKEN Brain Science Institute, Saitama, Japan). The generation of the lentiviral particles was performed as described in previous publications (Weber, Thomaschewski, Benten, & Fehse, 2012) and the protocol for the transduction is described in (Fuge et al., 2017). The novel CHO DP-12 cell line, stably expressing the FUCCI fusion proteins, is henceforth referred to as CHO DP-12 (FUCCI). The cells were expanded using multiple T-flasks in an incubator (37°C; 5% CO<sub>2</sub>) and the cells were transferred to a single-use Erlenmeyer baffled flask with a working volume of 40 ml (Corning). The incubator atmosphere (LT-XC; Kuhner, Switzerland) was controlled at 37°C, 5% CO<sub>2</sub>, and 85% humidity. Shaking speed was set at 200 rpm and 25 mm shaking diameter. Further expansion of cells was performed using multiple shake flasks and a cryobank was created.

## 2.2 | Automated and online flow cytometry

An automated and online flow cytometry (AFC) set-up was designed as follows. A needle (diameter: 1 mm, Medorex, Germany) was connected to the bioreactor representing an inline sampling port and a small tubing (diameter: 0.5 mm, length: 60 cm) was connected to the flow cytometer (Cytoflex, Beckman Coulter, Germany) instead of the sample needle. Sample shaking was turned off and backflushing after measurement was set to a minimum of 1 s to avoid contamination of the bioreactor. This set-up could be used to measure the fluorescence signals of the FUCCI system online and the samples were neither filtered nor stained before measurement. Furthermore, automated measurements with distinct time intervals or at distinct times were performed using the desktop automation software "perfect automation" (Version 2.7.1, available at <http://www.perfectautomation.com/>). Then, a flow of 60 µl/min was set for 6 min to flush the tube with fresh cultivation broth. The term online was defined according to Biechele et al. (2015) because the sampling time is low (approx. 10 min total) compared to the process dynamics (approx. 22 hr for cell cycle; Biechele, Busse, Solle, Scheper, & Reardon, 2015). Fifty thousand events were recorded at an appropriate flow rate and the system was turned to standby afterward.

### 2.2.1 | Quantification of FUCCI fluorescence with $I_{red}^n$

The flow cytometer measurements were analyzed as described in (Fuge et al., 2017). In brief, debris was excluded using SSC-A versus FSC-A and doublets were excluded with FSC-H versus FSC-A gating. mKO<sub>2</sub> (red, G1 phase) was measured using a 488 nm laser and a 585/42 filter and mVenus (green, S/G2/M phase) was quantified using the same laser and a 525/40 nm filter. The gains in both measurements were adjusted to 50 (arbitrary unit). Compensation (mVenus-24% mKO<sub>2</sub>, mKO<sub>2</sub>-42.5% mVenus) was necessary to reduce cross talk. mVenus positive cells were defined above a measured intensity of  $4 \times 10^4$  a.u. and mKO<sub>2</sub> positive cells above  $2 \times 10^4$  a.u., which was defined based on the autofluorescence of nontransduced CHO DP-12 cells. It was shown that the ratio of these fluorescence signals (viz.,  $I_{red}^n$ ) can be applied to estimate the cell cycle distribution of the culture (Fuge et al., 2017). Therefore, the number of mKO<sub>2</sub> positive cells is divided by the number of mKO<sub>2</sub> and mVenus positive cells

$$I_{red}^n[\%] = \frac{mKO_2^n}{mKO_2^n + mVenus^n} \quad (1)$$

It is a relative representation of the cell cycle distribution and (Fuge et al., 2017) identified the significant correlation of  $I_{red}^n$  with the cell cycle distribution of exponentially growing cells. Furthermore, the concept of  $I_{red}^n$  measurements was introduced for the estimation of the current growth rate of nonoscillating cultures. This study aims at an improved understanding of the cell cycle distributions and the application of  $I_{red}^n$  as a measure of the growth rate was not targeted. The calculation of  $I_{red}^n$  can be done directly using the flow cytometry

data. See the Supporting Information materials (Figure S1) for more information about the gating of the flow cytometer data.

## 2.3 | Cultivations

In this study, different cultivation concepts have been tested *in silico* to assess if they might induce cell cycle oscillations. A repeated-batch set-up and a (bolus) fed-batch were investigated. A continuous feeding strategy was used as a negative control for the fed-batch process.

### 2.3.1 | Preculture

A single-use Erlenmeyer baffled flask (40 ml; Corning) was inoculated with freshly thawed cryo-cultures ( $1 \times 10^7$  cells/ml). The incubator atmosphere and the expansion were as described in Generation of FUCCI-derived cell line derivatives. All cultivations were performed without antibiotics and serum.

### 2.3.2 | Repeated-batch cultivation

The cultivation of nonsynchronized CHO DP-12 (FUCCI) cells in a repeated-batch (see Möller et al., 2018) was performed in the bioreactor Medorex Vario 1000 (Medorex). The working volume at the beginning was 100 ml fresh medium (TC-42, Xell AG). The medium was supplemented with 0.1 mg/L LONG R3 IGF-1, 1 mM glutamine, and 200 nM methotrexate. The pH was controlled at 7.1 ( $\text{CO}_2$  or 0.5 M  $\text{Na}_2\text{CO}_3$ ), agitation at 400 rpm, temperature at 36.8°C. Headspace aeration of air was supplied at 10 ml/min and  $\text{CO}_2$  was added in the headspace for pH adjustment. Dissolved oxygen was controlled at 40% minimum and pure oxygen was sparged submersely if necessary. A total of  $2 \times 10^6$  cells/ml were inoculated and a partial medium exchange was performed every 22 hr to set the glucose and glutamine concentrations as calculated in the model-based study and to adjust the cell concentration to the predicted values. Therefore, part of the medium was removed and a freshly prepared medium was fed to the bioreactor. AFC measurements (Automated and online flow cytometry) were conducted every hour. Offline cell cycle measurements were conducted every 3 hr in the fourth batch.

### 2.3.3 | Fed-batch cultivation

The bioreactor set-up in the fed-batch cultivation was the same as in the repeated-batch experiment (Repeated-batch cultivation). The working volume was 150 ml fresh medium (supplemented as in Repeated-batch cultivation) and  $0.3 \times 10^6$  cells/ml were inoculated. The bolus feed (Chomacs basic feed, Xell AG, 111 mM glucose) was supplemented with 9 mM glutamine. 10% (based on current volume) of prewarmed feed was added every 24 hr, with the first feed after 48 hr cultivation time. In the negative control, the same quantity of the same feeding solution was supplied continuously using a syringe pump (AL1000; World Precision Instruments GmbH, Friedberg,

Germany) with a flow rate of 10% of the actual bioreactor volume supplied per day. The flow rate was adjusted each day to account for an increase in volume.

### 2.3.4 | Analytics

Concentrations of glucose ( $c_{\text{Glc}}$ ), glutamine ( $c_{\text{Gln}}$ ), and lactate ( $c_{\text{Lac}}$ ) were measured with the YSI 2900D (Yellow Springs Instruments) biochemistry analyzer. The concentration of ammonium ( $c_{\text{Amm}}$ ) was determined with an enzymatic test kit (AK00091; NZYTech, Portugal). The antibody ( $c_{\text{Ab}}$ ) was measured with biolayer interferometry (Octet RED; Pall ForteBio) with protein A biosensors (Pall ForteBio) in accordance with the manufacturer protocol. The cell concentration was measured with the particle counter Z2 (Beckman Coulter, described in (Castillo et al., 2012)) and with the gated single cells during the AFC (2.2.1). The flow-cytometer liquid flow was calibrated on the Z2 measurements. Viability was measured with the 4,6-diamidin-2-phenylindol (DAPI) method, as explained in (Möller et al., 2018) or with the Trypan Blue method. The cell cycle distribution was determined based on the distribution of DAPI stained DNA (Möller et al., 2018; Platas Barradas et al., 2015).

## 2.4 | Population-resolved model

A stochastic population-resolved model was adapted to predict a process for the induction of cell cycle-dependent oscillations based on the feeding strategy. The basis of the model is the division of the total cell population into four distinct cell cycle states ( $\Omega = [\text{G1}, \text{S}, \text{G2M}, \text{dead cells}]$ ). In each phase, a cell cycle-specific DNA replication rate and volumetric growth rate are modeled individually. Cell growth is based on the substrates glucose, glutamine and potentially lactate (Equations S4 and S5). Furthermore, the cell cycle-dependent metabolic regulations are included for glucose, glutamine, lactate, ammonium, and the antibody (Equations S6–S10). Möller et al. (2018) identified the formation of a putative autocrine factor and showed its interactions with the metabolism, which is also considered in the model (Equations S11–S13). The cell cycle-specificity is implemented with individual model parameter sets for all  $\Omega$ , that is G1, S, and G2/M-dependent parameters, allowing the description of cell cycle-dependent metabolic up- and downregulation. This approach has so far been applied to identify cell cycle dependencies such as increasing antibody productivity during the S-phase of CHO DP-12 cells (Möller et al., 2018). The model is set up as a single cell model simulating 1,000 cells with individual growth and metabolism in accordance with the cell cycle. The transition among different  $\Omega$  is described stochastically with Gaussian probability density functions (Equations S15–S17; Liu, Bi, Zeng, & Yuan, 2007). Furthermore, a random variation in the growth rate for each simulated cell is considered (Equations S2 and S3) to reflect the individual growth variability on the single-cell level. The concentration changes and growth progressions simulated for single cells are numerically integrated (Equation S18) and the simulation results are scaled to the experimental cell number (Equation S1) to reflect the bioprocess bulk behavior. A

detailed explanation and discussion of the model components can be found in the Supporting Information material and (Jandt et al., 2015; Möller et al., 2018).

### 2.4.1 | Process-induced cell cycle oscillations

In the model, the effective cell growth rate (Equation S5) is a function of the substrate concentrations including glutamine. This is modeled based on substrate-specific growth rates ( $k_i$ ) with Monod-like structures (Equation S4). Here, the focus is specifically on the contribution of the glutamine-dependent growth rate  $k_{\text{Gln}}$ , as depicted

$$k_{\text{Gln}} = \frac{c_{\text{Gln}}}{(K_{\text{Gln}} + c_{\text{Gln}})}. \quad (2)$$

$K_{\text{Gln}}$  describes the affinity of  $k_{\text{Gln}}$  to the glutamine concentration in the medium. It was observed in preliminary simulation studies that even small cell cycle dependencies of  $K_{\text{Gln}}$  would presumably lead to significant cell cycle fluctuations depending on the bulk glutamine profiles. In earlier studies, any potential cell cycle dependency of  $K_{\text{Gln}}$  was not targeted and thus it was assumed to be constant (Jandt et al., 2015; Möller et al., 2018). In this study, a cell cycle-dependent affinity of the cell growth to glutamine was considered and  $K_{\text{Gln}}$  in Equation ((2)) was extended with a dimensionless cell cycle-specific scaling factor  $K_{\text{Gln},\Omega}$  which gives

$$k_{\text{Gln}} = \frac{c_{\text{Gln}}}{(K_{\text{Gln}} \cdot K_{\text{Gln},\Omega} + c_{\text{Gln}})}. \quad (3)$$

The model extension phenomenologically reflects the strong impact of glutamine on the cell metabolism and biosynthesis (DeBerardinis & Cheng, 2010; Yang et al., 2016) and a changing cell response to the available glutamine during the cell cycle (Jandt et al., 2015; Möller et al., 2018; Son et al., 2013). The assumed cell cycle-dependent volumetric growth rate (Equation ((3))) would, in theory, lead to an accumulation of cells in defined cell cycle positions based on the glutamine profiles in the medium. This allows real synchronization, which would pose no contradiction to synchronization criteria defined by (Cooper, 1998a; Jandt et al., 2014). Note that this approach does not rely on specific restriction points and that cell cycle-dependent variations of  $K_{\text{Glc}}$  and  $K_{\text{Lac}}$  were not targeted. Here, the consideration of cell cycle-dependent growth rates with  $K_{\text{Gln},\Omega}$  was used to predict the potential influence of process strategies on the induction of cell cycle oscillations.

### 2.4.2 | Adaptation of model parameters

The model parameters were readapted to the experimental data of the repeated-batch and fed-batch process following the workflow described in the Supporting Information material and (Möller et al., 2018). In brief, the measured data were smoothed (Gaussian convolution,  $\delta = 3$  hr) to reduce the measurement noise. Then, the model parameters were adapted based on the filtered data using the

Nelder–Mead optimization algorithm (Nelder & Mead, 1965; Singer & Singer, 2004). The parameters were adapted stepwise (different objective functions, see Supplementary materials or (Möller et al., 2018)) and the obtained parameter sets are referred to as best-fit.

The cell cycle-specific parameters  $K_{\text{Gln},\Omega}$  were adapted on the offline cell cycle data of the repeated-batch process between 66 and 96 hr because very detailed time-resolved data of the cell cycle progression was available only between these time points.  $i_{\text{ed}}^n$  data were not used for parameter fitting, but for validation, as it should roughly correlate with the G1 phase distribution.

### 2.4.3 | Model parameter uncertainty quantification

To validate and evaluate the uncertainty of the model predictions, 50 independent parameter adaptations were performed starting from the best-fit. Due to the semistatistical nature of the model, each parameter adaptation differs. Therefore, the uncertainty of the model predictions was evaluated. The model was implemented in GNU C++ and the computational demand required to estimate the optimal parameter sets (500 iterations for each parameter optimization, 50 replicates total) is roughly between 10 and 20 CPU hr. Adaptations were performed on the High-Performance-Computer-Cluster at TUHH. The 10% and 90% percentiles of the simulated data were calculated based on the function “prctile” (MATLAB 2018a, exact mode; Langford, 2006).

## 3 | RESULTS AND DISCUSSION

It was investigated, whether and to which extent oscillations in the cell cycle distribution are induced in CHO DP-12 (FUCCI) cultures, depending on the feeding strategy. Oscillations were predicted using a population balance model derived from (Möller et al., 2018), assuming  $K_{\text{Gln},\text{G1}} \gg K_{\text{Gln},\text{S}} \approx K_{\text{Gln},\text{G2/M}}$  (see Equation ((3))) and supply of a regular feed pulse and the glutamine concentration oscillating above and below approx. 0.5 mM in the culture. This was confirmed with the following two types of experiments: First, a repeated-batch cultivation concept to study stable cell cycle oscillations was developed in silico and evaluated experimentally. Second, the induction of cell cycle fluctuations was predicted and validated in a (bolus) fed-batch, which was compared to a continuously supplied feed as negative control. Then, the model parameters were refined to the new available experimental data to minimize residual errors (for the parameter list, see Table S1). Note that, when keeping  $K_{\text{Gln},\Omega} = 1$  as in previous works, no oscillations occurred, as expected (data not shown).  $K_{\text{Gln},\Omega}$  were adapted to the detailed cell cycle data of the repeated-batch cultivation (Performed repeated-batch process) and evaluated on all cultivations.

### 3.1 | Stable oscillating repeated-batch

Repeated-batch cultures were shown to be advantageous for the study of cell cycle dependencies because overlaying effects, such as



**TABLE 1** Determined process parameters for a repeated-batch process with induced cell cycle oscillations

| Variable     |   |
|--------------|---|
| $C_{Gln,0}$  | 1 mM  |
| $C_{Gln,ME}$ | adjusted to restore $C_{Gln,0}$               |
| $V_{\%,ME}$  | 42%   |
| $t_{ME}$     | 22 hr   |
| $X_{v,0}$    | $2 \cdot 10^6 \frac{\text{cells}}{\text{ml}}$ |

substrate limitations and presumed metabolite inhibitions could be avoided (Möller et al., 2018). Furthermore, they offer a semicontinuous cultivation concept for long term studies (Kim, Bang, Kim, Jang, & Lee, 2016) and are used as a scale-down model for example perfusion processes (Chen, Wong, & Goudar, 2018; Wolf et al., 2018).

### 3.1.1 | Determined process parameters

The identification of the process parameters for the induction of cell cycle oscillations was based on the population-resolved model (see Population-resolved model). The initial glutamine concentration  $C_{Gln,0}$ , the glutamine concentration in the fresh medium ( $C_{Gln,ME}$ ), the percentage of replaced medium ( $V_{\%,ME}$ ) and the time points for medium exchange ( $t_{ME}$ ) were predicted using simulations based on their ability to induce cell cycle oscillations. The initial viable cell density ( $X_{v,0}$ ) was set to  $2 \times 10^6$  cells/ml based on former experiments (Möller et al., 2018). It was identified that a high oscillation of nonsynchronized cultures through repeated-batch experiments could be obtained for the cultivation parameters shown in Table 1.

These parameters enable the glutamine concentration to be between 1 and approximately 0.1 mM. After  $t_{ME}$ , part of the medium was replaced and  $C_{Gln,0}$  and  $X_{v,0}$  were restored at the beginning of each batch. Furthermore, the glucose concentration was designed to remain higher than 20 mM, so limitations and inhibitions could be prevented.

### 3.1.2 | Performed repeated-batch process

The suggested experiment was performed and the measured concentrations and online  $i_{red}^n$  signals are shown in Figure 1.

The adapted curves of the best-fit and the corresponding 10/90% quantiles are in good agreement with the measured data. The minimal and maximal values of the corresponding parameters and the parameters of the best-fit can be found in Table S1.

#### FUCCI fluorescence

As can be seen in Figure 1a,  $i_{red}^n$  starts to increase during the first 12 hr past inoculation and then decreases until the first medium exchange at 22 hr. After that, the amplitudes increase from 16% in batch 2 to a stable value of 30% in batch 3 and batch 4. The duration of one cell cycle oscillation was  $\approx 20$  hr, which is in good agreement

to the doubling time of CHO DP-12 cells of nonsynchronized shake flask cultivations (40 ml working volume) of  $20.82 \text{ hr} \pm 1.70 \text{ hr}$  ( $n = 29$ ; see Möller, Kuchemüller, Steinmetz, Koopmann, & Pörtner (2019)). The  $i_{red}^n$  oscillations are stable and not damped, which typically occurs during the cultivations of physically synchronized cell populations in substrate excess (Jandt et al., 2014). A higher glutamine concentration (Figure 1e) was fed after 88 hr of cultivation and  $i_{red}^n$  prolongs with an additional oscillation without any medium exchanges.

#### Cell cycle distribution

The G1 phase distributions of the offline-samples (Figure 1c) show a cell cycle synchronization between 41% and 72%, which is comparable to physical synchronization techniques, such as countercurrent elutriation (Platas Barradas et al., 2015). A small-time shift of the amplitude of approx. 2 hr, although not easily observable, exists between the oscillations in Figure 1a,c.

#### Cell growth

Cell growth was quantified using flow cytometry data (Figure 1b) and offline measurements (Figure 1d). The gated single cells show a steady growth of the cultures without any lag phases due to low glutamine concentrations. The same steady growth was measured after the higher concentrated feed pulse at 88 hr. The viability was higher than 96% for all measurements and cell death was not observed.

#### Glutamine and ammonium

The glutamine concentration (Figure 1e) was adjusted to the calculated starting concentration of approximately 1 mM and it decreased in every batch close to 0.1 mM. The uptake of glutamine was constant between different batches and no stagnation of the glutamine uptake was observed after each medium exchange. No growth interruptions were observed due to the intermittently low concentrations of glutamine.

The assumed cell cycle-dependent differences in the glutamine-related growth rate were implemented in the model with cell cycle-dependent Monod constants (Process-induced cell cycle oscillations; Equation ((3))). The model parameters were adapted and  $K_{Gln,\Omega}$  were found to be significantly different between different cell cycle phases, shown in Figure 2.

$K_{Gln,G1}$  is significantly higher than  $K_{Gln,S}$  and  $K_{Gln,G2M}$ , which describes a higher affinity to low glutamine concentrations with a reduced growth during the G1 and the S phase in comparison to the G2/M phase. The concentration of ammonium (Figure 1f) increases from batch to batch, but stays below 1.5 mM and did not reach typical inhibitory concentrations (Noh, Park, Lim, Kim, & Lee, 2017; Zeng, Deckwer, & Hu, 1998).

#### Glucose and lactate

The concentration of glucose (Figure 1g) was in excess and above 20 mM for the five investigated batches. No limitations and no putative inhibitions were observed. The consumption of glucose was

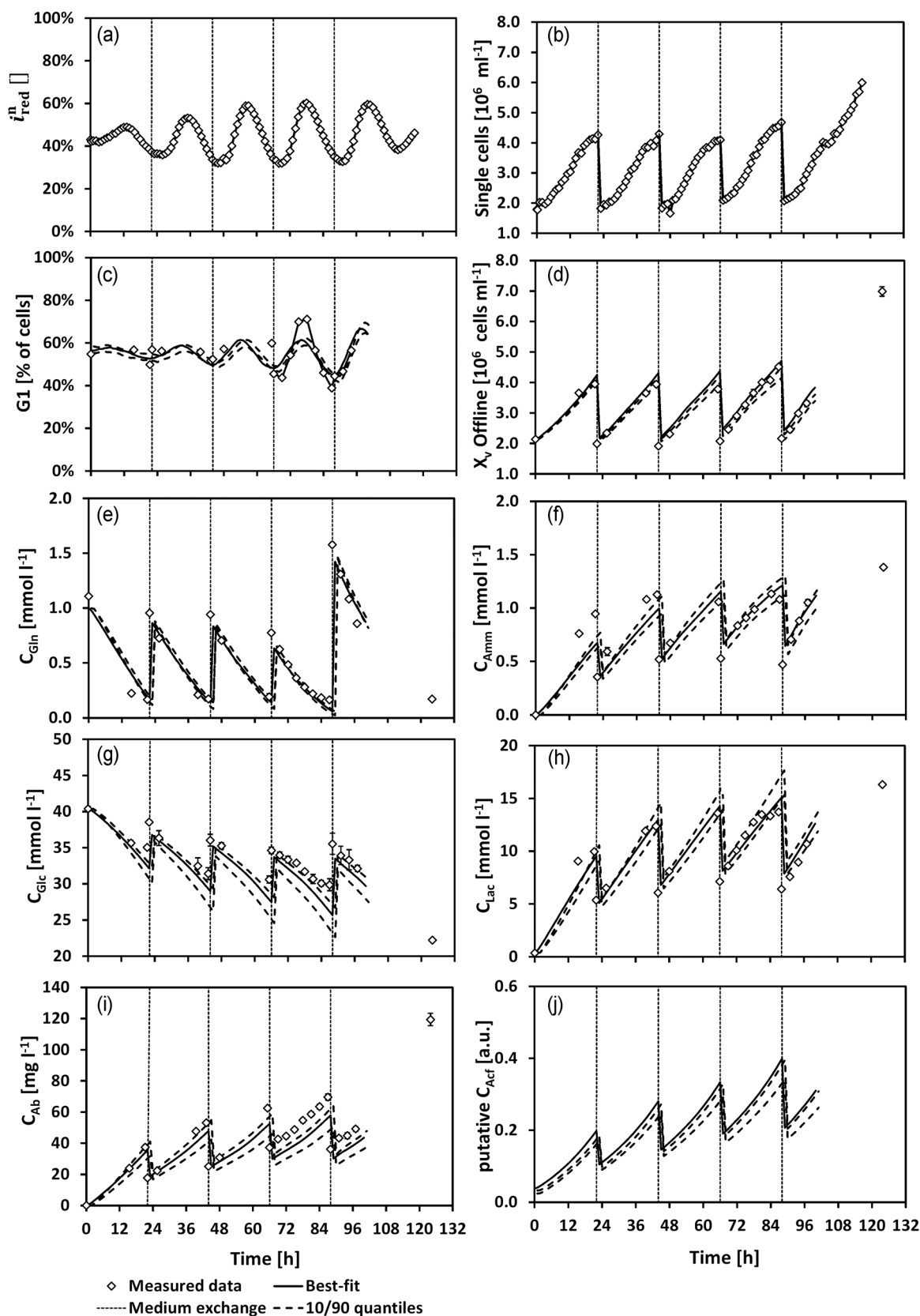


**FIGURE 1** Mean experimental results (diamonds) of the repeated-batch culture, solid line is the best-fit (see Population-resolved model), dashed line represents 10% and 90% quantiles of 50 independent parameter adaptations; error bars show the standard deviation of three technical measurements; exchange of the medium was performed every 22 hr (pointed line)

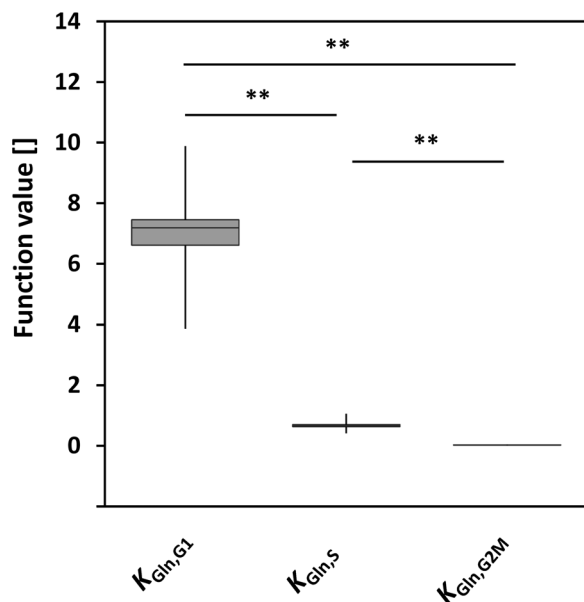


**FIGURE 2** Adapted cell cycle-specific growth constants for 50 independent parameter adaptations, two paired t test. \*\* = high significance ( $p < .001$ )

comparable in all batches. The lactate concentration increases strongly in the first batch from 0 to 10 mM and at the end of each batch. The lactate production per batch decreases from batch to batch. This effect could be coupled to a putative autocrine factor and was identified previously (Möller et al., 2018).

#### Antibody and putative autocrine factor

The antibody (Figure 1i) was formed constantly and was diluted with every feeding step, thus increasing batch-wise. The putative autocrine factor (Figure 1j) was simulated to be expressed constantly over the five batches, as described previously (Möller et al., 2018).

### 3.2 | Feeding-induced cell cycle oscillations

A fed-batch process for the induction of cell cycle synchronization was developed based on the population-resolved model (2.4). Fed-batch processes are predominantly applied in the biopharmaceutical industry and could be used to understand process-induced cell cycle dependencies in high cell density cultures (Pan, Dalm, Wijffels, & Martens, 2017; Zhu, 2012).

#### 3.2.1 | Determined process parameters

Similar to the repeated-batch set-up, a low-glutamine environment (supplied bolus-wise) was tested to induce cell cycle synchronization in fed-batch cultures. The proposed feeding strategy was based on the population-resolved model and prior studies for the model-assisted design of fed-batch strategies (Möller et al., 2018, 2019). Using the model-based approach, a cell cycle oscillation was predicted in fed-batch cultivations for the process parameters shown in Table 2.

**TABLE 2** Determined process parameters for a fed-batch process with induced cell cycle oscillations

| Variable       |                        |
|----------------|------------------------|
| $C_{Gln,Feed}$ | 9 mM                   |
| $C_{Glc,Feed}$ | 111 mM                 |
| $F_{Rate}$     | 10% of starting volume |
| $F_{Start}$    | 48 hr                  |

The glucose concentration in the feed ( $C_{Glc,F}$ ) was set to 111 mM based on the available medium. The feed rate ( $F_{Rate}$ ) and the start of feeding ( $F_{Start}$ ) were defined based on the availability of glutamine with estimated concentrations below 1 mM after 48 hr. The glutamine concentration in the feed ( $C_{Gln,Feed}$ ) was defined in a way that low-glutamine conditions comparable with the repeated-batch concept could be ensured.

#### 3.2.2 | Performed fed-batch process

The performed fed-batch is depicted in Figure 3 including the adapted best-fit of the population-resolved model and the 10/90% quantiles.

In general, modeling was only performed during the exponential and transition phase (until 168 hr) and not during the stationary (approx. 168–216 hr) and death phase ( $t > 216$  hr). The mechanisms of cell death, including apoptosis, necrosis, and cell lysis are not understood properly, even in a holistic way (Klein et al., 2015; Tabas & Ron, 2011). Moreover, the influence of these effects on the cell cycle is still unknown and was not targeted in this study (Chaiboonchoe et al., 2018; Hydbring, Malumbres, & Sicinski, 2016).

#### FUCCI fluorescence

$i_{red}^n$  (see Figure 3a) is stable at approx. 42% for the first 72 hr of cultivation without any oscillations. After the second feed pulse at 72 hr, it starts to oscillate slowly with a difference in  $i_{red}^n$  of 8% between 72 and 96 hr. After that, an oscillation of the  $i_{red}^n$  signals with an increasing peak height until 132 hr was observed. After the feed pulse at 144 hr,  $i_{red}^n$  increases again but the oscillation stops after 168 hr and  $i_{red}^n$  constantly increases further up to 100%. No oscillations were observed in the negative control (orange line) where  $i_{red}^n$  increased on average comparable to the bolus fed-batch. Overall, the concentrations (Figure 3e–h) and the cell numbers (Figure 3b,d) of the negative control (continuous feeding) were in the same range as the bolus fed-batch process.

#### Cell cycle distribution

The cell cycle distribution was purely modeled (Figure 3c) and the oscillations of simulated G1 content are comparable to the  $i_{red}^n$  measurements. The increase in the average  $i_{red}^n$  (comparable to the negative control) was no part of the modeling and only oscillation of  $i_{red}^n$  is reflected in the G1 phase distribution.



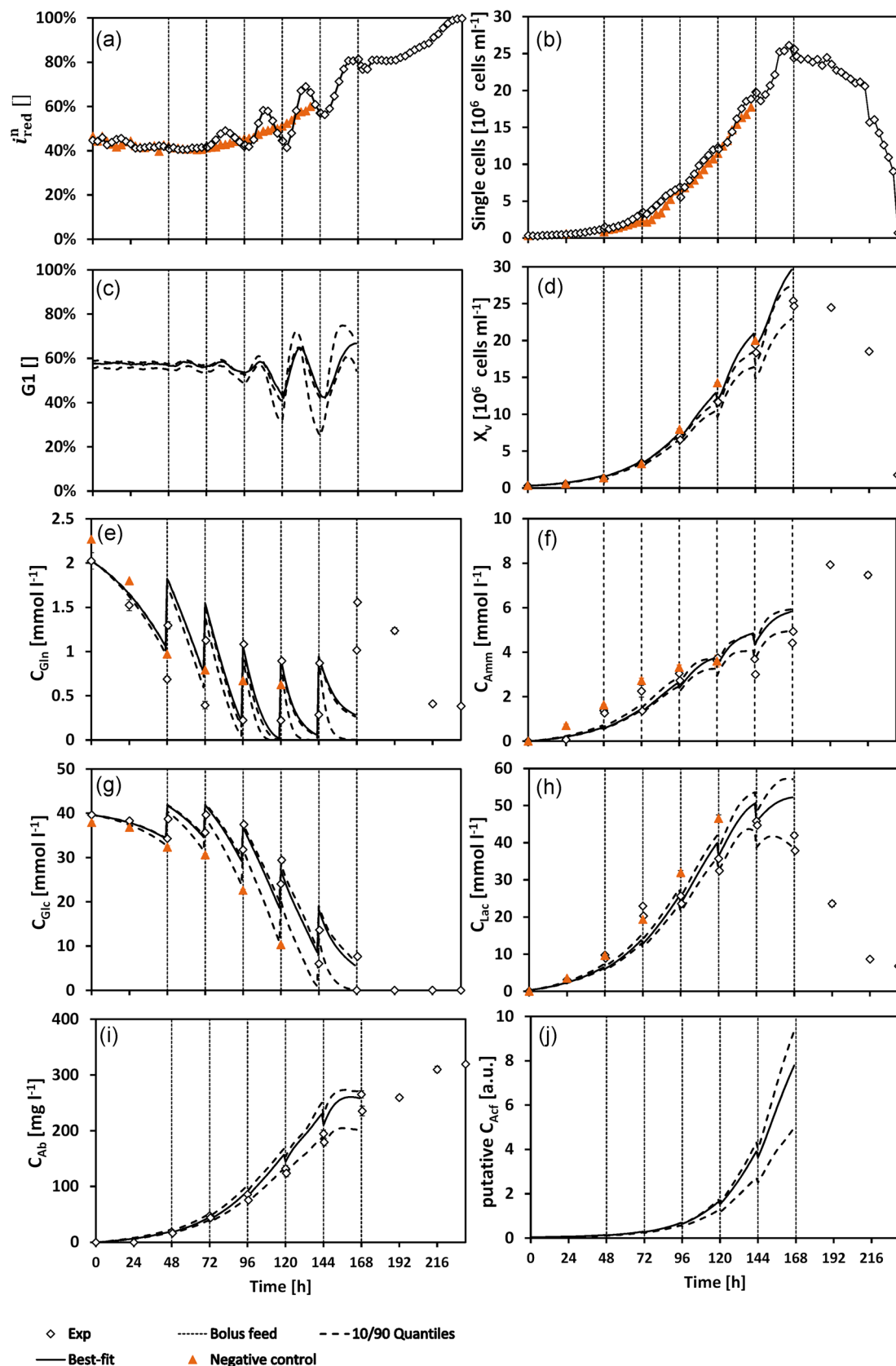


**FIGURE 3** Mean experimental results (diamonds) of the fed-batch culture, solid line is the best-fit (see Population-resolved model), dashed line represents 10% and 90% quantiles of 50 independent parameter adaptations; error bars show the standard deviation of three technical measurements; feeding was performed every 24 hr (pointed line) with a start at 48 hr. Negative control with continuous feeding in orange [Color figure can be viewed at [wileyonlinelibrary.com](http://wileyonlinelibrary.com)]

### Cell growth

The single-cell concentration determined with gating (Figure 3b) increases from  $0.3 \times 10^6$  cells/ml up to  $25 \times 10^6$  cells/ml. The growth phases including the death phase after approximately 192 hr could be seen using the AFC approach. The offline-determined cell densities show similar numbers and the best-fit reflects the measurements sufficiently. Cell lysis could be identified during the death phase with decreasing particle sizes and therefore a decrease in gated cells (Kroll, Stelzer, & Herwig, 2017). The negative control exhibited similar growth behavior as the pulse-feed cultivation.

### Glutamine and ammonium

The glutamine concentration (Figure 3e) decreased from 2 to 0.5 mM after 48 hr and was then fed every 24 hr as a bolus. It did not fall below 0.2 mM and was not limiting during the fed-batch cultures. After 144 hr, the glutamine uptake was slower and no glutamine was taken up between 144 and 168 hr. The overall glutamine profile of the negative control was comparable to the averaged trend of that seen in the pulse fed-batch cultivation. The model reflects the glutamine profiles sufficiently, but the glutamine uptake at the beginning (48–72 hr) was partly underestimated. The change in the glutamine uptake rates (i.e., high at the beginning and low at the end) was simulated with acceptable variations. The 10/90% quantiles are relatively wide, which is based on the simulation of starvation effects near to 0 mM glutamine and part of the readapted curves reach the starvation earlier than others. The concentration of ammonium (3f) increases up to 4 mM until 168 hr, for which no inhibitory effects were described in the literature (Hassell, Gleave, & Butler, 1991; Hayter et al., 1991; Zeng et al., 1998).

### Glucose and lactate

The concentration of glucose (Figure 3g) decreases below the starting value of 40 mM and was depleted between 144–168 hr, which corresponds to the transition of the cell culture into the stationary growth phase. The concentration of lactate (Figure 3h) increases constantly up to 45 mM and lactate is taken up after glucose is consumed. This metabolic lactate switch itself and its regulations remain unclear and were not targeted in this study (Zalai et al., 2015; Zagari, Jordan, Stettler, Broly, & Wurm, 2013).

### Antibody and putative autocrine factor

The antibody concentration (Figure 3i) increased constantly during the fed-batch process and was comparable to former studies (Möller et al., 2019). The putative autocrine factor (Figure 3j) was estimated to rise.

## 3.3 | Discussion

### 3.3.1 | Glutamine-dependent cell cycle synchronization

The role of glutamine in cell metabolism is still being investigated and discussed (reviewed in DeBerardinis & Cheng, 2010). On the one hand, glutamine is taken up during the glutaminolysis and provides energy to the TCA cycle, which is required during cell proliferation

(Lunt & Vander Heiden, 2011). On the other hand, it is seen as a nitrogen donor during nucleotide biosynthesis and is therefore essential in cell cultures (Tardito et al., 2015; Tohyama et al., 2016). However, the uptake of glutamine is significantly higher than needed for biosynthesis and an ineffective metabolism comparable to the Warburg effect is described in tumor cells (DeBerardinis & Cheng, 2010; DeBerardinis et al., 2007). Previously, the glutamine metabolism was found to be significantly cell cycle-dependent in the mammalian cell lines CHO K1, AGE1<sub>AAT</sub> and CHO DP-12 (Jandt et al., 2015; Möller et al., 2018). In this study, partial cell cycle synchronization was identified based on the process strategy with glutamine concentrations in the oscillation-inducing range of approximately 0.2–1.0 mM. This effect is likely to be biologically related to an upregulation of the glutamine uptake/metabolism during the G1/S phase, for example, due to an increased glutamine demand during cell growth and DNA synthesis (Möller et al., 2018; Son et al., 2013). The highly significant differences in the adapted model parameter  $K_{Gln,\Omega}$  (Figure 2) describe this effect. Thus, a strong cell cycle control based on glutamine or glutamine-dependent intermediates in CHO DP-12 (FUCCI) cells is postulated.  $K_{Gln,G2/M}$  was significantly reduced, which indicates a low glutamine dependency of the G2/M phase.

### 3.3.2 | Absence of cell cycle arrest

The cell cycle itself is the basis of cell proliferation and it is strongly regulated in mammalian cells (Kohrman & Matus, 2017; Lopez-Mejia & Fajas, 2015). The main regulation of the cell cycle is based on the cyclin-dependent kinases (CDK) 4 and CDK6 (Gelbert et al., 2014). They form a heterodimer (CDK4/6) and are involved in cell cycle control (review in Otto & Sicinski, 2017). In general, cell cycle arrests with changing metabolic regulations and cell death were identified for the depletion of nutrients (Roth et al., 2002; Saqcena et al., 2013; Zhang et al., 2014). This effect could be linked to the decrease of intracellular cyclin levels due to pathways associated with response to amino acid deprivation (Dey et al., 2010; Du et al., 2015). Furthermore, Cooper (2003) and Jandt et al. (2014) questioned cell cycle synchronization methods using cell cycle arrest by, for example, chemical cell cycle blockage in general.

Here, no overall reduction of the growth rate with apparent dysregulations, example cell death, cell cycle arrest, or extensive metabolic changes was observed. Cell cycle synchronization was achieved based on the process strategy with the previously described low-glutamine concentrations supplied bolus wise. No growth inhibition/limitation with lag-phases or induction of cell death/lysis have been identified neither in the repeated-batch nor fed-batch process (excluding death phase). Metabolic dysregulations or changing uptake or formation rates were not observed. In both processes, no suppression of the antibody production by the process was observed, even for low-glutamine conditions. Furthermore, metabolic changes were not seen if the model simulations including the 10/90% quantiles are compared to the measured data (comparable to Möller et al., 2018). The proposed processes and methods could, therefore, be applied to gain an improved

understanding of cell cycle-enriched populations and their dynamics in physiologically synchronized cultures.

### 3.3.3 | $i_{red}^n$ for online cell cycle measurements

The online monitoring and control of mammalian cell culture processes are mostly based on bulk signals. Historically, pH or dissolved oxygen (DO) has been related to changes in the cell metabolism and process control strategies (e.g., feeding on OUR) were developed based on these measurements (Hu & Aunins, 1997; Jiang, Chen, & Xu, 2018; Romn et al., 2018). Even novel measurement concepts in the process analytical technology initiative mostly measure bulk compositions and relate this information to cellular regulations and effects. Exemplary, online glucose measurements (Zhang et al., 2015) or RAMAN spectroscopy (Berry et al., 2016; Matthews et al., 2018) are discussed in the literature. These measurement concepts are very useful to understand processes in a holistic way, but only partially useful to gain an understanding of population heterogeneity with changing cell metabolism.

This study shows the application of AFC for the quantification of cell population-based phenomena using  $i_{red}^n$ . A correlation to the cell cycle of individual cells was identified during the exponential growth phase. However, the overall increase of  $i_{red}^n$  at the end of the cultivation could not be purely linked to the cell cycle distributions. Cell starvation at the end of the cultivations could include the transition of the cells into a quiescent state (sometimes referred to as G0 phase) including changes in the protein expression, degradation, and cell cycle regulation (Münzer et al., 2015). We observed that mKO<sub>2</sub>-hCdt1(30/120) accumulates during late-stage growth and the stationary phase, for which (Tomura et al., 2013) presumed an accumulation due to the transition of the cell population into a G0 phase. Even though the pure existence of a G0 phase has been disputed at all (Cooper, 1998b), the accumulation of mKO<sub>2</sub>-hCdt1(30/120) cells, including an increase in  $i_{red}^n$ , correlates with metabolic deactivation and cell death.

## 4 | CONCLUSION

The impact of different cultivation and feeding strategies on the induction of cell cycle oscillations was investigated in nonsynchronized processes with antibody-producing CHO DP-12 cells. The cells were genetically modified to stably express the FUCCI system and an automated flow cytometry set-up was developed to measure the cell cycle indicator  $i_{red}^n$  online. First, a repeated-batch process was assessed based on a population-resolved model. Stable cell cycle oscillations were measured in five repeated batches (22 hr each). Second, it was evaluated how a bolus feeding strategy induces cell cycle synchronizations. Interestingly, significant metabolic differences in the cell cycle-dependent glutamine metabolism were identified, which are the basis of process-induced cell cycle synchronization. This provides a novel approach to understand and control cell cycle regulations and thus to either intentionally triggers cell cycle synchronizations in cell culture

processes or, on the other hand, avoid unwanted fluctuations due to inappropriate (bolus) feeding strategies. Further studies will focus on the direct control of  $i_{red}^n$  with an adaptation of the population-resolved model into a process control system.

## ACKNOWLEDGMENTS

This study was partially funded by the Deutsche Forschungsgemeinschaft (DFG, Grant ZE 542/9R1) and German Federal Ministry of Education and Research (BMBF, Grant 031B0222). KR received funding from DFG Sonderforschungsbereich SFB841 (SP2). We thank the FACS-Sorting Core Facility at the UKE for their service and help regarding flow cytometry. The authors declare that there are no conflicts of interest.

## ORCID

Johannes Möller  <http://orcid.org/0000-0001-9546-055X>

Ralf Pörtner  <http://orcid.org/0000-0003-1163-9718>

Uwe Jandt  <http://orcid.org/0000-0001-8221-5176>

## REFERENCES

- Berry, B. N., Dobrowsky, T. M., Timson, R. C., Kshirsagar, R., Ryll, T., & Wiltberger, K. (2016). Quick generation of raman spectroscopy based in-process glucose control to influence biopharmaceutical protein product quality during mammalian cell culture. *Biotechnology Progress*, 32(1), 224–234.
- Biechle, P., Busse, C., Solle, D., Scheper, T., & Reardon, K. (2015). Sensor systems for bioprocess monitoring. *Engineering in Life Sciences*, 15(5), 469–488.
- Castillo, A. E., Fuge, G., Jandt, U., & Zeng, A.-P. (2012). Growth kinetics and validation of near-physiologically synchronized HEK293s cultures. *Nature Protocols*, 7, 839–849.
- Chaiboonchoe, A., Khraiweh, B., Murali, C., Baig, B., El-Awady, R., Tarazi, H., & Amin, A. (2018). Safranin induces dna double-strand breakage and ER-stress-mediated cell death in hepatocellular carcinoma cells. *Scientific Reports*, 8(1), 16951.
- Chen, C., Wong, H. E., & Goudar, C. T. (2018). Upstream process intensification and continuous manufacturing. *Current Opinion in Chemical Engineering*, 22, 191–198.
- Chusainow, J., Yang, Y. S., Yeo, J. H., Toh, P. C., Asvadi, P., Wong, N. S., & Yap, M. G. (2009). A study of monoclonal antibody-producing cho cell lines: What makes a stable high producer? *Biotechnology and Bioengineering*, 102(4), 1182–1196.
- Cooper, S. (1998a). Mammalian cells are not synchronized in g1-phase by starvation or inhibition: Considerations of the fundamental concept of g1-phase synchronization. *Cell Proliferation*, 31(1), 9–16.
- Cooper, S. (1998b). On the proposal of a G0 phase and the restriction point. *The FASEB Journal*, 12(3), 367–373.
- Cooper, S. (2003). Rethinking synchronization of mammalian cells for cell cycle analysis. *Cellular and Molecular Life Sciences CMLS*, 60(6), 1099–1106.
- Cooper, S., & Gonzalez-Hernandez, M. (2009). Experimental reconsideration of the utility of serum starvation as a method for synchronizing mammalian cells. *Cell Biology International*, 33(1), 71–77. <https://doi.org/10.1016/j.cellbi.2008.09.009>
- DeBerardinis, R. J., & Cheng, T. (2010). Qas next: The diverse functions of glutamine in metabolism, cell biology and cancer. *Oncogene*, 29(3), 313.

- DeBerardinis, R. J., Mancuso, A., Daikhin, E., Nissim, I., Yudkoff, M., Wehrli, S., & Thompson, C. B. (2007). Beyond aerobic glycolysis: Transformed cells can engage in glutamine metabolism that exceeds the requirement for protein and nucleotide synthesis. *Proceedings of the National Academy of Sciences*, 104(49), 19345–19350.
- Deglinerti, A., Etoc, F., Ozair, M. Z., & Brivanlou, A. H. (2016). Chapter six - self-organization of spatial patterning in human embryonic stem cells. In P. M. Wassarman (Ed.), *Essays on developmental biology, Part A* (pp. 99–113). Academic Press *Current Topics in Developmental Biology*.
- Dey, S., Baird, T. D., Zhou, D., Palam, L. R., Spandau, D. F., & Wek, R. C. (2010). Both transcriptional regulation and translational control of atf4 are central to the integrated stress response. *Journal of Biological Chemistry*, 285(43), 33165–33174.
- Du, Z., Treiber, D., McCarter, J. D., Fomina-Yadlin, D., Saleem, R. A., McCoy, R. E., & Reddy, P. (2015). Use of a small molecule cell cycle inhibitor to control cell growth and improve specific productivity and product quality of recombinant proteins in cho cell cultures. *Biotechnology and Bioengineering*, 112(1), 141–155.
- Fuge, G., Hong, Y., Riecken, K., Zeng, A.-P., & Jandt, U. (2017). Cho cells engineered for fluorescence read out of cell cycle and growth rate in real time. *Biotechnology Progress*, 33(5), 1408–1417.
- Gelbert, L. M., Cai, S., Lin, X., Sanchez-Martinez, C., del Prado, M., Lallena, M. J., & de Dios, A. (2014). Preclinical characterization of the cdk4/6 inhibitor LY2835219: In-vivo cell cycle-dependent/independent anti-tumor activities alone/in combination with gemcitabine. *Investigational New Drugs*, 32(5), 825–837. <https://doi.org/10.1007/s10637-014-0120-7>
- Hassell, T., Gleave, S., & Butler, M. (1991). Growth inhibition in animal cell culture. *Applied Biochemistry and Biotechnology*, 30(1), 29–41.
- Hayter, P. M., Curling, E. M. A., Baines, A. J., Jenkins, N., Salmon, I., Strange, P. G., & Bull, A. T. (1991). Chinese hamster ovary cell growth and interferon production kinetics in stirred batch culture. *Applied Microbiology and Biotechnology*, 34(5), 559–564.
- Hu, W.-S., & Aunins, J. G. (1997). Large-scale mammalian cell culture. *Current Opinion in Biotechnology*, 8(2), 148–153.
- Hydbring, P., Malumbres, M., & Sicinski, P. (2016). Non-canonical functions of cell cycle cyclins and cyclin-dependent kinases. *Nature Reviews Molecular Cell Biology*, 17(5), 280.
- Imura, T., & Lee, J.-W. (2017). Unveiling a rhythmic regulatory mode hidden in developmental tissue growth by fluorescence live imaging-based mathematical modeling. *Journal of Oral Biosciences*, 59(1), 6–11.
- Jandt, U., Platas Barradas, O., Pörtner, R., & Zeng, A. (2014). Mammalian cell culture synchronization under physiological conditions and population dynamic simulation. *Applied Microbiology and Biotechnology*, 98(10), 4311–4319. <https://doi.org/10.1007/s00253-014-5553-6>
- Jandt, U., Platas Barradas, O., Pörtner, R., & Zeng, A.-P. (2015). Synchronized mammalian cell culture: Part II – population ensemble modeling and analysis for development of reproducible processes. *Biotechnology Progress*, 31(1), <https://doi.org/10.1002/btpr.2006>
- Jang, J., Wang, Y., Lalli, M. A., Guzman, E., Godshalk, S. E., Zhou, H., & Kosik, K. S. (2016). Primary cilium-autophagy-nrf2 (pan) axis activation commits human embryonic stem cells to a neuroectoderm fate. *Cell*, 165(2), 410–420.
- Jiang, R., Chen, H., & Xu, S. (2018). pH excursions impact cho cell culture performance and antibody n-linked glycosylation. *Bioprocess and Biosystems Engineering*, 41(12), 1731–1741.
- Kim, C. L., Bang, Y. L., Kim, Y. S., Jang, J. W., & Lee, G. M. (2016). Alleviation of proteolytic degradation of recombinant human bone morphogenetic protein-4 by repeated batch culture of chinese hamster ovary cells. *Process Biochemistry*, 51(8), 1078–1084.
- Klein, T., Heinzl, N., Kroll, P., Brunner, M., Herwig, C., & Neutsch, L. (2015). Quantification of cell lysis during cho bioprocesses: Impact on cell count, growth kinetics and productivity. *Journal of Biotechnology*, 207, 67–76.
- Kohrman, A. Q., & Matus, D. Q. (2017). Divide or conquer: Cell cycle regulation of invasive behavior. *Trends in Cell Biology*, 27(1), 12–25. <https://doi.org/10.1016/j.tcb.2016.08.003>
- Kroll, P., Stelzer, I. V., & Herwig, C. (2017). Soft sensor for monitoring biomass subpopulations in mammalian cell culture processes. *Biotechnology Letters*, 39(11), 1667–1673.
- Langford, E. (2006). Quartiles in elementary statistics. *Journal of Statistics Education*, 14(3).
- Liu, Y.-H., Bi, J.-X., Zeng, A.-P., & Yuan, J.-Q. (2007). A population balance model describing the cell cycle dynamics of myeloma cell cultivation. *Biotechnology Progress*, 23(5), 1198–1209.
- Lopez-Mejia, I. C., & Fajas, L. (2015). Cell cycle regulation of mitochondrial function. *Current Opinion in Cell Biology*, 33, 19–25.
- Lunt, S. Y., & Vander Heiden, M. G. (2011). Aerobic glycolysis: Meeting the metabolic requirements of cell proliferation. *Annual Review of Cell and Developmental Biology*, 27(1), 441–464.
- Matthews, T. E., Smelko, J. P., Berry, B., Romero-Torres, S., Hill, D., Kshirsagar, R., & Wiltberger, K. (2018). Glucose monitoring and adaptive feeding of mammalian cell culture in the presence of strong autofluorescence by near infrared raman spectroscopy. *Biotechnology Progress*, 34(6), 1574–1580.
- Möller, J., Korte, K., Pörtner, R., Zeng, A.-P., & Jandt, U. (2018). Model-based identification of cell-cycle-dependent metabolism and putative autocrine effects in antibody producing cho cell culture. *Biotechnology and Bioengineering*, 115(12), 2996–3008.
- Möller, J., Kuchemüller, K. B., Steinmetz, T., Koopmann, K. S., & Pörtner, R. (2019). Model-assisted design of experiments as a concept for knowledge-based bioprocess development. *Bioprocess and Biosystems Engineering*, 42(5), 867–882.
- Münzer, D. G., Ivarsson, M., Usaku, C., Habicher, T., Soos, M., Morbidelli, M., & Mantalaris, A. (2015). An unstructured model of metabolic and temperature dependent cell cycle arrest in hybridoma batch and fed-batch cultures. *Biochemical Engineering Journal*, 93, 260–273.
- Nelder, J. A., & Mead, R. (1965). A simplex method for function minimization. *The Computer Journal*, 7(4), 308–313.
- Newman, R. H., & Zhang, J. (2008). Fucci: Street lights on the road to mitosis. *Chemistry and Biology*, 15(2), 97–98.
- Noh, S. M., Park, J. H., Lim, M. S., Kim, J. W., & Lee, G. M. (2017). Reduction of ammonia and lactate through the coupling of glutamine synthetase selection and downregulation of lactate dehydrogenase-a in cho cells. *Applied Microbiology and Biotechnology*, 101(3), 1035–1045.
- Otto, T., & Sicinski, P. (2017). Cell cycle proteins as promising targets in cancer therapy. *Nature Reviews Cancer*, 17(2), 93.
- Pan, X., Dalm, C., Wijffels, R. H., & Martens, D. E. (2017). Metabolic characterization of a cho cell size increase phase in fed-batch cultures. *Applied Microbiology and Biotechnology*, 101(22), 8101–8113.
- Patel, N. A., Anderson, C. R., Terkildsen, S. E., Davis, R. C., Pack, L. D., Bhargava, S., & Clarke, H. R. (2018). Antibody expression stability in cho clonally derived cell lines and their subclones: Role of methylation in phenotypic and epigenetic heterogeneity. *Biotechnology Progress*, 34(3), 635–649.
- Platas Barradas, O., Jandt, U., Becker, M., Bahnmann, J., Pörtner, R., & Zeng, A.-P. (2015). Synchronized mammalian cell culture: Part I – a physical strategy for synchronized cultivation under physiological conditions. *Biotechnology Progress*, 31(1), <https://doi.org/10.1002/btpr.1944>
- Romn, R., Farris, M., Camps, M., Martinez-Monge, I., Comas, P., Martinez-Espelt, M., & Cair, J. (2018). Effect of continuous feeding of CO<sub>2</sub> and pH in cell concentration and product titers in hifn producing hek293 cells: Induced metabolic shift for concomitant consumption of glucose and lactate. *Journal of Biotechnology*, 287, 68–73.
- Roth, E., Oehler, R., Manhart, N., Exner, R., Wessner, B., Strasser, E., & Spittler, A. (2002). Regulative potential of glutamine relation to glutathione metabolism. *Nutrition*, 18(3), 217–221.

- Sakaue-Sawano, A., Kurokawa, H., Morimura, T., Hanyu, A., Hama, H., Osawa, H., & Miyawaki, A. (2008). Visualizing spatiotemporal dynamics of multicellular cell-cycle progression. *Cell*, 132(3), 487–498.
- Saqcena, M., Menon, D., Patel, D., Mukhopadhyay, S., Chow, V., & Foster, D. A. (2013). Amino acids and mtor mediate distinct metabolic checkpoints in mammalian g1 cell cycle. *PLOS One*, 8(8).
- Scarcelli, J. J., Hone, M., Beal, K., Ortega, A., Figueroa, B., Starkey, J. A., & Anderson, K. (2018). Analytical subcloning of a clonal cell line demonstrates cellular heterogeneity that does not impact process consistency or robustness. *Biotechnology Progress*, 34(3), 602–612.
- Schoors, S., Bruning, U., Missiaen, R., Queiroz, K. C., Borgers, G., Elia, I., & Carmeliet, P. (2015). Fatty acid carbon is essential for dntp synthesis in endothelial cells. *Nature*, 520(7546), 192.
- Singer, S., & Singer, S. (2004). Efficient implementation of the Nelder–Mead search algorithm. *Applied Numerical Analysis and Computational Mathematics*, 1(2), 524–534. <https://doi.org/10.1002/anac.200410015>
- Son, J., Lyssiotis, C. A., Ying, H., Wang, X., Hua, S., Ligorio, M., & Kimmelman, A. C. (2013). Glutamine supports pancreatic cancer growth through a kras-regulated metabolic pathway. *Nature*, 496(7443), 101.
- Tabas, I., & Ron, D. (2011). Integrating the mechanisms of apoptosis induced by endoplasmic reticulum stress. *Nature Cell Biology*, 13(3), 184.
- Tardito, S., Oudin, A., Ahmed, S. U., Fack, F., Keunen, O., Zheng, L., & Gottlieb, E. (2015). Glutamine synthetase activity fuels nucleotide biosynthesis and supports growth of glutamine-restricted glioblastoma. *Nature Cell Biology*, 17(12), 1556.
- Tohyama, S., Fujita, J., Hishiki, T., Matsuura, T., Hattori, F., Ohno, R., & Fukuda, K. (2016). Glutamine oxidation is indispensable for survival of human pluripotent stem cells. *Cell Metabolism*, 23(4), 663–674.
- Tomura, M., Sakaue-Sawano, A., Mori, Y., Takase-Utsugi, M., Hata, A., Ohtawa, K., & Miyawaki, A. (2013). Contrasting quiescent g0 phase with mitotic cell cycling in the mouse immune system. *PLOS One*, 8(9):e73801.
- Vcelar, S., Jadhav, V., Melcher, M., Auer, N., Hrdina, A., Sagmeister, R., & Borth, N. (2018). Karyotype variation of cho host cell lines over time in culture characterized by chromosome counting and chromosome painting. *Biotechnology and Bioengineering*, 115(1), 165–173.
- Weber, K., Thomaschewski, M., Benten, D., & Fehse, B. (2012). Rgb marking with lentiviral vectors for multicolor clonal cell tracking. *Nature Protocols*, 7(5), 839.
- Wolf, M. K., Lorenz, V., Karst, D. J., Souquet, J., Broly, H., & Morbidelli, M. (2018). Development of a shake tube-based scale-down model for perfusion cultures. *Biotechnology and Bioengineering*, 115(11), 2703–2713.
- Yang, L., Achreja, A., Yeung, T.-L., Mangala, L. S., Jiang, D., Han, C., & Negrath, D. (2016). Targeting stromal glutamine synthetase in tumors disrupts tumor microenvironment-regulated cancer cell growth. *Cell Metabolism*, 24(5), 685–700.
- Zagari, F., Jordan, M., Stettler, M., Broly, H., & Wurm, F. M. (2013). Lactate metabolism shift in cho cell culture: The role of mitochondrial oxidative activity. *New Biotechnology*, 30(2), 238–245.
- Zalai, D., Koczka, K., Parta, L., Wechselberger, P., Klein, T., & Herwig, C. (2015). Combining mechanistic and data-driven approaches to gain process knowledge on the control of the metabolic shift to lactate uptake in a fed-batch cho process. *Biotechnology Progress*, 31(6), 1657–1668.
- Zeng, A.-P., Deckwer, W.-D., & Hu, W.-S. (1998). Determinants and rate laws of growth and death of hybridoma cells in continuous culture. *Biotechnology and Bioengineering*, 57(6), 642–654.
- Zhang, A., Tsang, V. L., Moore, B., Shen, V., Huang, Y.-M., Kshirsagar, R., & Ryll, T. (2015). Advanced process monitoring and feedback control to enhance cell culture process production and robustness. *Biotechnology and Bioengineering*, 112(12), 2495–2504.
- Zhang, J., Fan, J., Venneti, S., Cross, J. R., Takagi, T., Bhinder, B., & Thompson, C. B. (2014). Asparagine plays a critical role in regulating cellular adaptation to glutamine depletion. *Molecular Cell*, 56(2), 205–218.
- Zhu, J. (2012). Mammalian cell protein expression for biopharmaceutical production. *Biotechnology Advances*, 30(5), 1158–1170.

## SUPPORTING INFORMATION

Additional supporting information may be found online in the Supporting Information section.

**How to cite this article:** Möller J, Bhat K, Riecken K, Pörtner R, Zeng A-P, Jandt U. Process-induced cell cycle oscillations in CHO cultures: Online monitoring and model-based investigation. *Biotechnology and Bioengineering*. 2019;116:2931–2943. <https://doi.org/10.1002/bit.27124>